Non-Gaussian fluctuations in electromagnetic radiation scattered by a random phase screen. II. Application to dynamic scattering in liquid crystal

1975 J. Phys. A: Math. Gen. 8 392

(http://iopscience.iop.org/0305-4470/8/3/011)

J. Phys. A: Math. Gen., Vol. 8, No. 3, 1975. Printed in Great Britain.

Non-Gaussian fluctuations in electromagnetic radiation scattered by a random phase screen
II. Application to dynamic scattering in a liquid crystal

P N Pusey and E Jakeman

Royal Radar Establishment, Malvern, Worcestershire WR14 3PS, UK

Received 14 August 1974

Abstract. We have studied experimentally the statistical, spatial coherence and temporal coherence properties of non-Gaussian fluctuations in light scattered by a thin layer of liquid crystal (MBBA) in its dynamic scattering state. The results are consistent with the deep phase-screen theory developed in the previous paper I. With 20 V applied to the sample, experimental values of the parameters of the model are: mean square phase deviation $\overline{\phi^2} = 45{\cdot}6 \pm 8{\cdot}0\,\text{rad}^2$, phase correlation length $\xi = 2{\cdot}63 \pm 0{\cdot}24\,\mu\text{m}$ and phase coherence time $2{\cdot}2 \pm 0{\cdot}2$ s. Indications are found that, while phase fluctuations in the emergent wavefront are probably dominant, amplitude fluctuations are not entirely negligible. It is argued, however, that the effects of amplitude fluctuations on the values of the above parameters are probably quite small. Taking a broader view, our results confirm that, in many scattering experiments, detailed information concerning the scattering process can be obtained from measurements in the non-Gaussian regime (illuminated region of sample comparable in size to scatterer structure), which is not available from studies in the Gaussian regime (illuminated region $\gg$ scatterer structure).

1. Introduction

In the previous paper (Jakeman and Pusey 1975, to be referred to as I), we have considered the theory of non-Gaussian fluctuations in electromagnetic radiation scattered by a random phase screen. In this paper we describe an experimental investigation of non-Gaussian fluctuations in light scattered by the nematic liquid crystal MBBA in its 'dynamic scattering' state, interpreting our results in terms of this theory.

In 1968 Heilmeier *et al* discovered that, if an electric field (DC or low frequency AC) was applied across a layer (typically 10–100 μm thick) of a nematic liquid crystal having negative dielectric anisotropy, above a certain voltage threshold (typically 5–8 V) the layer changed from a relatively transparent state to an opaque state causing strong light scattering. This effect, named 'dynamic scattering', is due to refractive index fluctuations caused by hydrodynamic turbulence induced in the liquid crystal by the application of the field. In 1969 Deutsch and Keating investigated the dependence of the scattered light intensity on incident and final polarizations and scattering angle, and gave a theoretical analysis of their results. They considered the situation where the liquid crystal was initially aligned in some direction by eg rubbing the transparent conducting plates enclosing the layer. With no applied electric field, thermal motions cause displacements of the molecules about their mean direction leading to small refractive index fluctuations and thus relatively weak scattering (see eg Orsay liquid

crystal group 1969, Haller and Litster 1970). Electrohydrodynamic turbulence, however, causes larger refractive index fluctuations and thus stronger scattering. Deutsch and Keating considered propagation of electromagnetic radiation normal to the liquid crystal layer and showed that, on passage through a region of uniform angular displacement of the optic axis, the radiation suffers, in general, alteration in both amplitude and phase. At applied voltages significantly above threshold, a typical path through the liquid crystal will intercept several turbulence eddies and transmitted radiation will therefore, in general, undergo both random time-dependent phase retardations and random time-dependent amplitude modulations. If, however, we consider incident radiation normal to the plane of the liquid crystal layer, having polarization parallel to the alignment direction, then, at least for relatively small orientational fluctuations, phase retardations are dominant in transmitted radiation having the same polarization as the incident radiation (HH scattering) whereas amplitude fluctuations are more important for transmitted radiation of the orthogonal polarization (HV scattering). Thus the ratio of the intensity of HV scattering to that of HH scattering provides a measure of the relative importance of amplitude and phase fluctuations in dynamic scattering (and hence, indirectly, a measure of the magnitude of the induced orientational fluctuations). Deutsch and Keating found that, for applied voltages not too far above threshold and scattering angles not too near zero, this ratio was small ($\lesssim 0{\cdot}1$) indicating that, at least in the HH scattering configuration, the liquid crystal behaves as a phase screen. Dynamic scattering in a liquid crystal thus appears to be a convenient system in which to test the predictions of the theory presented in I.

It should be mentioned, however, that the arguments given above apply only to sufficiently thin films where it is assumed that each 'ray' of radiation passes through the sample virtually undeviated in direction, simply picking up phase (and perhaps amplitude) modulations. With thicker films significant angular deviations may occur within the sample. This gives rise to the possibility that different 'rays', having suffered different phase shifts early in their passage through the sample, may interfere at some point in the exit face of the sample providing additional amplitude fluctuations (see also Briggs 1966, Salpeter 1967). It is possible that this source of amplitude fluctuations is not negligible in our experiments. For example there are indications that the light beam is broadened somewhat on passage through the sample (see § 3.2). Nevertheless, in what follows we shall analyse our data assuming the simple phase screen to be a good model of dynamic scattering in the HH configuration. We do this partly because it is difficult to quantify the effect of amplitude fluctuations and partly because the simple phase-screen theory seems to provide a good description of our data. However, the effects of possible amplitude fluctuations will be discussed in more detail in § 4.

It should also be emphasized that, since a given 'ray' will usually intercept several turbulence eddies on passage through the sample, the phase correlation length ξ, determined in these experiments, does not provide a direct measure of the turbulence correlation length, a quantity of perhaps more fundamental interest. In general, the former length can be expected to be smaller than the latter (see, for example, Little and Hewish 1966). However, as the nature of the turbulence is altered by, say, changes in the applied voltage, changes in ξ and the turbulence correlation length can be expected to be in the same direction. It remains an unsolved problem to relate the quantities $\overline{\phi^2}$ and ξ obtained from our experiments directly to the fundamental mechanisms of electrohydrodynamically induced refractive index fluctuations.

Many of the effects investigated in this paper are visible to the naked eye. Imagine a laser beam focused by a lens onto a liquid crystal layer (see figure 1). With no voltage

applied to the liquid crystal the beam passes through virtually unperturbed apart from a small attenuation due to scattering by the natural thermal fluctuations. On application of a voltage significantly above the threshold voltage, however, the whole transmitted beam is spread out to an angular width of some tens of degrees, forming on a screen behind the sample a characteristic flickering speckle pattern. As the applied voltage is increased the rate of motion of this pattern increases, reflecting increasingly rapid turbulence within the sample. At about 20 V the motion of the pattern starts to become too rapid to be resolved by eye, corresponding to a coherence time of about 50 ms. If the diameter of the beam at the sample is fairly large, say 1 mm, the speckle pattern at 20 V averaged over a few speckles (or a few coherence times) has a fairly uniform appearance. This corresponds to the Gaussian regime, discussed in I, arising from the contributions of many facets in the transmitted phase front. As the diameter of the beam at the sample is reduced, the speckle size (conventional coherence area) increases as expected. In addition, however, large streaks of light appear, superimposed on the speckle pattern. These streaks, the non-Gaussian fluctuations associated with individual facets of the phase front, have the appearance of random 'lighthouse' beams. In general they cover many speckles and move relatively slowly. Indeed, at 20 V, an individual streak may have a lifetime of a second or so. After observing such effects by eye, it comes as no surprise that detailed measurements (§ 3) show the non-Gaussian fluctuations to have a spatial correlation length and coherence time much greater than those of the Gaussian fluctuations.

In fact, the relatively slow time scale of the non-Gaussian fluctuations constitutes a major disadvantage of the liquid crystal as a model phase screen. In order to obtain adequate statistical accuracy in the measurements, long experimental run-times are required. Our aim in this work was simply to achieve statistical accuracy good enough to provide a reasonable first test of the theory. Future work, at the expense of tedious experimentation, will perhaps provide a more detailed comparison of experiment and theory.

From I, the basic theoretical equations for the mean intensity, second intensity moment and spatial and temporal intensity correlation functions of light scattered by a deep phase screen are (I: equations (18), (21), (26), (32) and (52)):

$$\langle I(\theta,t)\rangle \propto \frac{W_0^2\xi^2}{\overline{\phi^2}}\exp\left(-\frac{k^2\xi^2\sin^2\theta}{4\overline{\phi^2}}\right) \tag{1}$$

$$\frac{\langle I^2(\theta,t)\rangle}{\langle I(\theta,t)\rangle^2} = 2\left(1-\frac{\xi^2}{W_0^2}\right)+\frac{\xi^2\overline{\phi^2}}{4W_0^2}\exp\left(\frac{k^2\xi^2\sin^2\theta}{4\overline{\phi^2}}\right) \tag{2}$$

$$\begin{aligned}\frac{\langle I(\theta,t)I(\theta',t)\rangle}{\langle I(\theta,t)\rangle\langle I(\theta',t)\rangle} &= \left(1-\frac{\xi^2}{W_0^2}\right)\left[1+\exp\left(-\frac{k^2W_0^2v^2}{4}\right)\right]\\ &\quad+\frac{\xi^2\overline{\phi^2}}{W_0^2}\left(\frac{J_1(\frac{1}{2}k\xi v)}{(\frac{1}{2}k\xi v)}\right)^2\exp\left(\frac{k^2\xi^2}{16\overline{\phi^2}}(u^2+2v^2)\right)\end{aligned} \tag{3}$$

$$\begin{aligned}\frac{\langle I(\theta,t)I(\theta,t+\tau)\rangle}{\langle I(\theta,t)\rangle^2} &= \left(1-\frac{\xi^2}{W_0^2}\right)\{1+\exp[2\overline{\phi^2}(\sigma(\tau)-1)]\}\\ &\quad+\frac{\xi^2}{W_0^2\{1-[\overline{\phi^2}\sigma(\tau)/(2+\overline{\phi^2})]^2\}}\exp\left(\frac{k^2\xi^2\sigma(\tau)\sin^2\theta}{2\overline{\phi^2}(1+\sigma(\tau))}\right).\end{aligned} \tag{4}$$

Here:

W_0 is the beam radius at the liquid crystal at the $1/e^2$ intensity point;
ξ is the phase correlation length;
$\overline{\phi^2}$ is the mean square phase deviation;
$k = 2\pi/\lambda$ is the magnitude of the wavevector of the light, λ being its wavelength;
θ, θ' are the angles, with respect to the normal, of the detectors (figure 1);
$v = \sin\theta - \sin\theta'$;
$u = \sin\theta + \sin\theta'$;
$\sigma(\tau)$ is the one-position temporal correlation function of the transmitted phase at the exit face of the sample, τ being the correlation delay time.

Note that in these equations $\sin\theta$ and $\sin\theta'$ always appear as the products $k\sin\theta$ and $k\sin\theta'$. These latter quantities are invariant under changes of refractive index. In interpreting our results, therefore, refraction effects are automatically accounted for if we consider k, θ and θ' in air (essentially *in vacuo*).

In the next section, we give details of the optical arrangement and data processing procedures. In § 3 the results of the measurements are presented and discussed. Various types of measurement were made. Firstly (§ 3.1) we made a preliminary investigation of the polarization and angular dependence of the mean scattered intensity (equation (1)). This confirmed the results of Deutsch and Keating (1969) and established that, at an applied voltage of 20 V, phase fluctuations were dominant in the HH scattering configuration, and the spatial correlation function of the transmitted phase approximated joint-Gaussian. In the HH configuration, measurements were then made of the single-interval statistics (§ 3.2, and equation (2)) and the spatial (§ 3.3 and equation (3)) and temporal (§ 3.4 and equation (4)) coherence properties of the scattered radiation. Overall agreement between experiment and theory was gratifying. The parameters characterizing the phase-screen behaviour of the liquid crystal were mean square phase shift $\overline{\phi^2} = 45{\cdot}6 \pm 8{\cdot}0\ \text{rad}^2$ and phase correlation length $\xi = 2{\cdot}63 \pm 0{\cdot}24\ \mu\text{m}$.

The fact that $\overline{\phi^2}^{1/2}$ is found to be greater than 2π indicates that, under the conditions of our experiment, the sample behaves as a *deep* phase screen. Thus after passage through the liquid crystal sample there should be nothing recognizable as a 'straight-through' beam (I, equation (17)). As mentioned above, this is indeed the situation observed by eye. To use a different terminology, this situation corresponds to strong multiple scattering. (For single scattering, as described by the first Born approximation, most of the incident radiation passes through the sample without being scattered. The degree of attenuation of the straight-through beam thus provides a direct measure of the importance of multiple scattering. Absence of a recognizable straight-through beam indicates strong multiple scattering.) There has been some success in describing the dynamic scattering process for thin layers of certain liquid crystal materials at low applied voltages in terms of single-scattering theories (Bertolotti *et al* 1971, 1972). Such theories do not apply to the work described in this paper.

2. Experimental details

Figure 1 shows a top view of the basic layout for the experiments to be described. The light source was a Spectra Physics model 119 single-mode helium–neon laser of output power less than about 100 μW at wavelength $\lambda = 6328$ Å. The electric field vector of the laser radiation was rotated into the horizontal plane. The liquid crystal

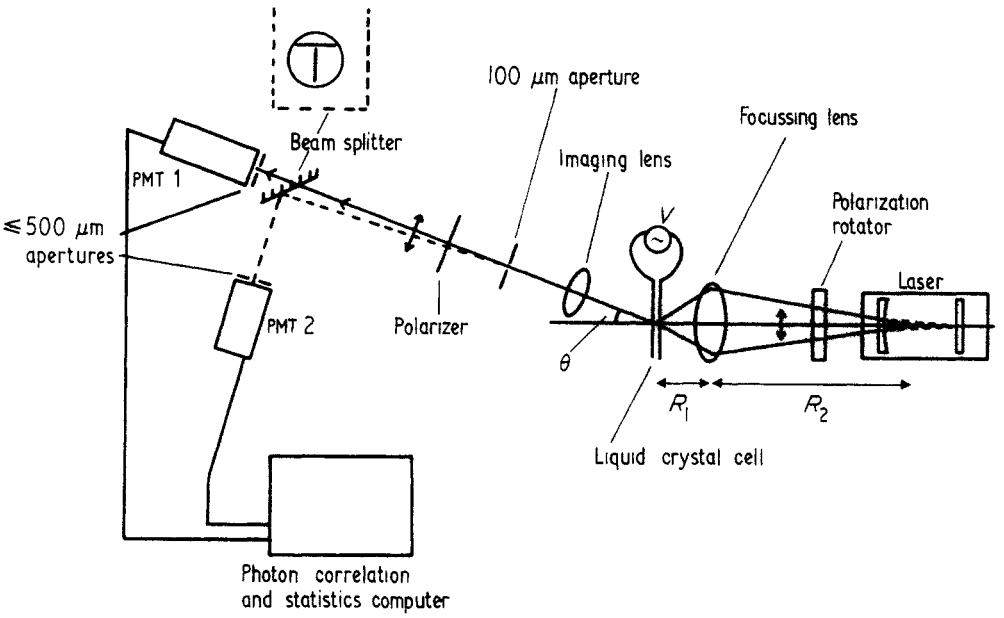

Figure 1. Experimental arrangement of components (top view). The inset shows the front view of the beam splitter which was adjusted (see text) so that scattered light detected by PMT 2 was reflected from the unmasked region at the intersection of the two strips of tape. The arrows indicate horizontal polarization directions of the incident and scattered radiation.

(MBBA) was sandwiched between tin-oxide coated glass plates, using 50 μm mylar spacers. The cell was sealed with epoxy resin. Experimental results were found to be reproducible for this sample over the period of the investigation, more than one year (see, however, § 4). The liquid crystal was aligned by rubbing the plates prior to cell assembly and the alignment direction was always in the horizontal plane (the plane of the diagram). A 50 Hz AC field could be applied across the sample. The laser beam was focused onto the sample using a lens of either 5 or 10 cm focal length which could be translated along the laser beam to allow the diffraction-limited waist of the laser beam to be positioned at the sample. The radius W of this waist (at the intensity $1/e^2$ points) was varied by altering the lengths R_1 and R_2 (figure 1) and was calculated from the equation (see eg Kogelnik and Li 1966):

$$W = \frac{2R_1\lambda}{\pi\phi R_2}, \tag{5}$$

where ϕ, the full divergence of the laser beam, was found to be 0·0089 rad by measuring the fraction of direct laser intensity transmitted by a circular aperture of known dimension. Values of R_2 ranged from 25 to 50 cm, giving W's in the range 5 to 30 μm.

In many, but not all, cases the scattered light was imaged (1 : 1 magnification) by a lens of focal length 5 cm onto a 100 μm diameter circular aperture in order to minimize detection of light multiply reflected by the glass plates. The scattered light then passed through a polarizer. For all measurements except the average intensity measurements to be described in § 3.1 the polarizer was set to pass light of horizontal polarization corresponding to the HH configuration discussed in § 1. ITT FW130 photomultiplier

tubes were used as detectors. They were preceded by 6328 Å dielectric filters to eliminate non-laser light and circular apertures of diameter less than 500 μm to ensure spatial coherence of the scattered light at the detectors. Background count rates with the laser beam blocked were typically less than 50 photocounts per second. For the maximum value of W_0 ($\simeq 30$ μm) and typical distance between the imaging aperture and detector of about 50 cm or more, the spatial coherence factor at the detectors was calculated to be of the order of 0·99 (see, eg Jakeman *et al* 1970, Koppel 1971), so that spatial coherence was virtually complete.

For two-detector experiments, a half-silvered mirror was placed roughly at 45° in front of PMT 1. This mirror could be translated perpendicular to the scattered radiation, and also vertically. Its orientation could also be changed about horizontal and vertical axes. On the face of the mirror were two strips of 0·5 mm black tape, as indicated in the inset of figure 1. There was a gap of about 0·5 mm between the vertical and horizontal strips. The apparent separation between the two detectors was changed as follows: first the mirror was moved a known distance perpendicular to the scattered light. Then, while observing the counting rate of PMT 2, the orientation of the mirror was adjusted (generally by a small amount) so that the scattered light detected by PMT 2 was always reflected from the (unmasked) point of intersection of the two strips of tape. This procedure appeared to give an error in the apparent angular position of PMT 2 with respect to that of PMT 1 of less than 0·02° (see figures 10 and 11). For larger separations ($\gtrsim 9°$) between the two detectors, the beam splitter was removed, and PMT 2 was simply placed in the scattered radiation field next to PMT 1.

The photomultiplier tubes were followed by conventional standardizing electronics, and photocount statistics and correlations were computed by a 'Malvern' K 7023 photon correlation and probability analyser†, whose operation is described in more detail, at appropriate points in the next section. (See, also, Jakeman (1974) and Oliver (1974) for recent discussions of the theory and practice of photon correlation.)

3. Results and discussion

3.1. Intensity measurements

Before embarking on the main subject of interest in this work, namely a study of photoelectron count (photocount) statistics and correlations, a few preliminary measurements were made of average intensity as a function of scattering angle and applied voltage. Photocounts were simply accumulated for 100 s to give an estimate, accurate to a few per cent, of the mean scattered intensity for the particular experimental configuration under study. In order to simplify experimental procedure, the imaging lens and aperture were not used in this preliminary study. However the counting rate with no applied field in the sample was less than 1/10 that with the field on, for all the data of figure 2, indicating that the magnitude of stray scattered light was small.

Figure 2 shows a semi-log plot of scattered intensity against $\sin^2\theta$, for applied voltages $V = 12$ V, 20 V and 50 V. Both the polarized HH (in the plane of figure 1) and depolarized HV scattered components were measured. At $V = 12$ V, the depolarized scattered light was much less intense than the polarized component, by a factor as great as 30 at some angles. There is, however, significant departure from the predictions of equation (1) for the polarized component (equation 1 predicts a straight line on this semi-log plot).

† Precision Devices and Systems, Malvern.

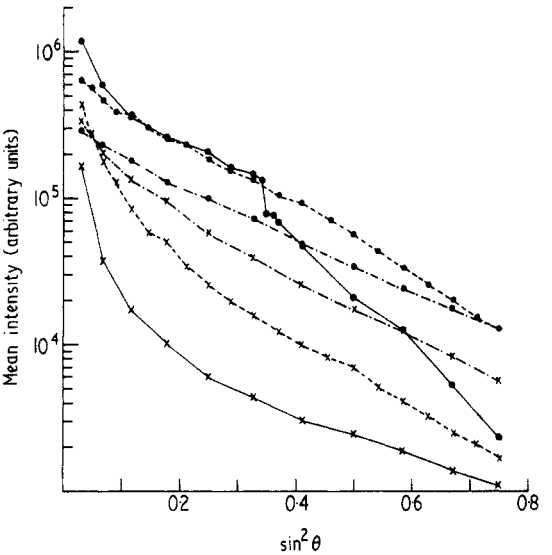

Figure 2. Mean scattered intensity as a function of scattering angle θ for horizontal (●) and vertical (×) polarizations of scattered radiation (horizontal incident polarization). Full curve, applied voltage $V = 12$ V; broken curve, $V = 20$ V; chain curve, $V = 50$ V.

This indicates, presumably, that random electrohydrodynamic turbulence is not fully developed in the liquid crystal at this voltage. At $V = 20$ V, the depolarized component is stronger, indicating that amplitude fluctuations in the transmitted electric field are becoming increasingly important (see § 1). However, the angular dependence of the polarized component, due largely to phase fluctuations, is in much better agreement with equation (1). Nevertheless there is still evidence of a change of slope at around $\theta = 40°$, due probably to residual structure in the turbulence. At $V = 50$ V, the polarized component is fitted well by a straight line, at least for $\theta > 25°$. However, the depolarized component is now much stronger, being only a factor of two or so less in intensity than the polarized component.

In view of these data, we felt the best operating voltage for our remaining experiments to be 20 V, where equation (1) is approximately valid, and the effects of the amplitude fluctuations are still relatively small. It should be noted, however, that at this voltage for $\theta \lesssim 20°$ the ratio of depolarized to polarized components increases as $\theta \to 0$, so that interpretation of experimental data in terms of a simple phase-screen model must be questionable in this region.

Figure 3 shows measurements of the intensities of the polarized and depolarized components as a function of voltage at $\theta = 30°$. As V increases the two intensities approach each other, indicating increasingly large orientational fluctuations of the liquid crystal molecules.

3.2. Single-interval statistics

Equation (2) gives the theoretical behaviour of the second intensity moment for a simple phase screen. In this section we describe the experimental dependence of the second moment on three variables, the illuminated area πW_0^2 at the screen, θ, the scattering angle, and V, the applied voltage for our liquid crystal sample.

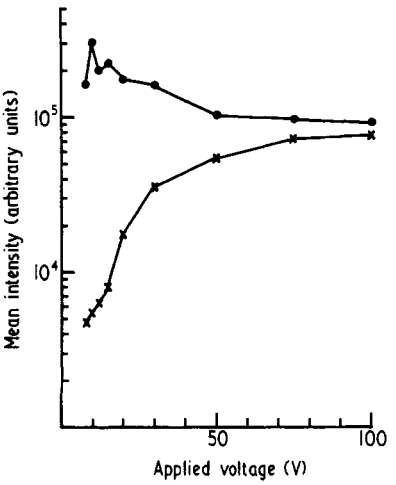

Figure 3. Dependence of mean intensity on applied voltage at scattering angle $\theta = 30°$. ●, Polarized (HH); ×, depolarized (HV).

The measurements were made using a single detector (PMT 1 in figure 1). The correlation computer was operated in the 'photon statistics' mode, which determines an experimental estimate of the probability $P(n)$ that n photocounts are detected in a sampling interval of duration T. From $P(n)$ several normalized factorial moments

$$n^{[m]} \equiv \frac{\Sigma_{n=0}^{\infty} n(n-1)\ldots(n-m+1)P(n)}{\langle n\rangle^m} \tag{6}$$

were calculated. *Whatever the form of the intensity statistics*, it can be shown that the $n^{[m]}$ are equal to the normalized moments of the intensity distribution (see, eg Mandel 1959, Pike 1969, Cantrell 1970). Thus $n^{[2]}$ is an experimental estimate of $\langle I^2\rangle/\langle I\rangle^2$. Sample times T ranged from 5 to 10 μs, much shorter than the coherence time of the light under study (>1 ms), so that temporal integration effects were negligible. Photon counting rates were typically $5\times10^4\ s^{-1}$, large enough to render negligible the effect of the background count rate, but small enough that dead-time effects were also unimportant. The dead-time of the electronics was about 50 ns. Two or three experimental runs of duration about 2 min each were typically performed. Without precise knowledge of the shape of the temporal correlation function in the non-Gaussian regime, accurate estimates of the experimental uncertainty in $P(n)$ cannot be made. However, taking the coherence time of the light to be 200 ms (figure 12), simple qualitative arguments predict the error in the second moment to be, for the parameters given above, greater than $(120/0{\cdot}2)^{-1/2}\times100\,\% \simeq 4\,\%$ for a single experimental run (see eg Jakeman *et al* 1971). Thus for several runs, the experimentally determined error of about 5 % (figures 6 and 8) is reasonable.

First we discuss the dependence of $n^{[2]}$ on the area of the liquid crystal layer illuminated by the laser beam. After coarse adjustment of the lengths R_1 and R_2 (see figure 1), the speckle pattern of the scattered light was allowed to fall on a screen, and the focusing lens position was adjusted for maximum speckle size (minimum illuminated area) as judged by eye. Final adjustment was made by measuring $n^{[2]}$ for various small displacements of the lens. The optimum position was taken to be that which gave the largest value of $n^{[2]}$. In principle the illuminated area for this optimum position is πW^2

where the beam waist W is given by equation (5). (It can be shown that the value of W is not affected by the insertion, perpendicular to the beam direction, of half-planes of different refractive index such as the glass plates enclosing the sample.) In practice, for the reasons mentioned in § 1, the laser beam will be broadened somewhat on passage through the sample. Thus the actual beam waist W_0 at the exit face of the sample, the quantity of interest for comparison of our results with the theory (equations (1)–(4)), will be somewhat larger than W. An estimate of the magnitude of this difference is obtained from figure 4 where experimental values of $(n^{[2]}-2)^{-1/2}$ are plotted against W for a range of R_1 and R_2 at scattering angle $\theta = 21{\cdot}6°$. To within experimental error, the data fit a straight line as predicted by equation (2). In contrast to equation (2), this line does not intercept zero, but tends to the value $W = -3 \pm 1$ μm as $(n^{[2]}-2)^{-1/2} \to 0$.

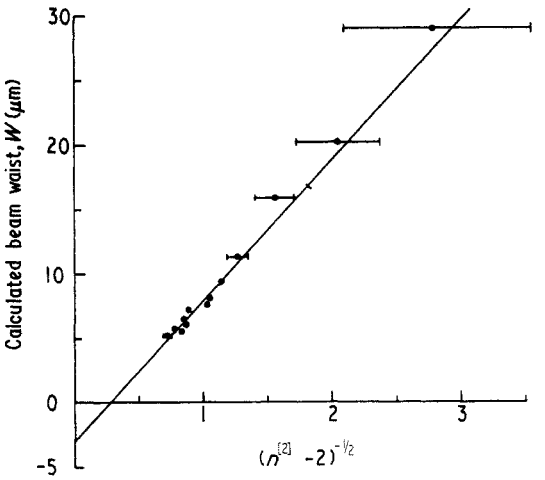

Figure 4. Plot of calculated beam waist W (equation (5)) against $(n^{[2]}-2)^{-1/2}$ for $\theta = 21{\cdot}6°$, $V = 20$ V. Intercept on the y axis yields the beam-spreading parameter' x.

This suggests that W_0, the actual beam waist at the exit face of the sample, is 3 μm greater than W, the value calculated from equation (5). In the remainder of this paper, therefore, we take

$$W_0 = W + x, \tag{7}$$

where the 'beam-spreading parameter' x has the value 3 μm. In figure 5 the data of figure 4 are replotted in a different form: $n^{[2]}$ is plotted against $(\pi W_0^2)^{-1}$. Straight-line behaviour is observed, as predicted by equation (2), and the Gaussian value of 2 is approached as the illuminated area is increased.

Figure 6 shows a semi-log plot of $n^{[2]}-2$ against $\sin^2\theta$ for a calculated beam waist W of 8·29 μm. According to equation (2) the data should lie nearly on a straight line and this is found to be the case within experimental error. In analysing these data we neglect the two lowest angle data points for which $\theta < 20°$, for reasons discussed in § 3.1. Assuming the beam-spreading parameter x to be 3 μm ($W_0 = 11{\cdot}29$ μm), the data can be well fitted by equation (2) with $\xi = 2{\cdot}63 \pm 0{\cdot}03$ μm and $\overline{\phi^2} = 45{\cdot}57 \pm 6$. For interest we also fitted the data taking $W_0 = 9{\cdot}29$ μm (ie $x = 1$ μm). This gave a curve almost indistinguishable from the first (figure 6) with $\xi = 2{\cdot}39$ μm and $\overline{\phi^2} = 37{\cdot}51$. Thus interpretation of the data is quite sensitive to the assumed value of W_0. Combining

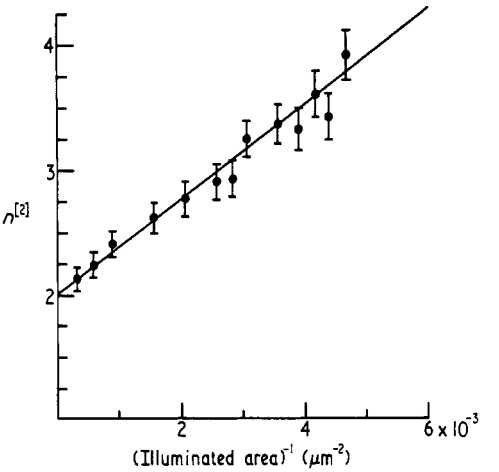

Figure 5. Dependence of normalized second intensity moment $n^{[2]}$ on reciprocal of area of sample illuminated. The full line is the theoretical prediction (equation (2)) with $\theta = 21{\cdot}6°$, $\xi = 2{\cdot}63$ μm and $\overline{\phi^2} = 45{\cdot}57$ rad^2.

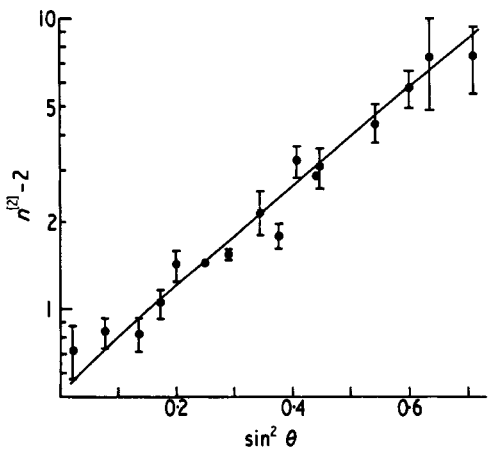

Figure 6. Angular dependence of the second intensity moment at $V = 20$ V, $W_0 = 11{\cdot}29$ μm. The full line is equation (2), with $\xi = 2{\cdot}63$ μm, $\overline{\phi^2} = 45{\cdot}57$ rad^2.

statistical errors and errors due to the uncertainty in W_0 the data of figure 6 are in agreement with $W_0 = 11{\cdot}29 \pm 2$ μm, $\xi = 2{\cdot}63 \pm 0{\cdot}24$ μm and $\overline{\phi^2} = 45{\cdot}57 \pm 8{\cdot}00$. The technique is thus seen to be very sensitive in determining ξ but rather less sensitive so far as $\overline{\phi^2}$ is concerned. If W_0 had been known accurately, ξ would have been determined to within 1% and $\overline{\phi^2}^{1/2}$ to within 7%, even for these data of limited accuracy.

Figure 7 shows a plot of $n^{[2]}$ against applied voltage at $\theta = 21{\cdot}6°$, $W_0 = 11{\cdot}29$ μm. We will not discuss these data in any detail except to say that qualitatively the behaviour is as expected. At high voltages the spatial scale of the turbulence, and hence the phase correlation length ξ, is expected to be small and the Gaussian value $n^{[2]} = 2$ is obtained. At lower voltages non-Gaussian effects become appreciable and $n^{[2]}$ increases rapidly as the threshold voltage (~ 7 V) for dynamic scattering is approached.

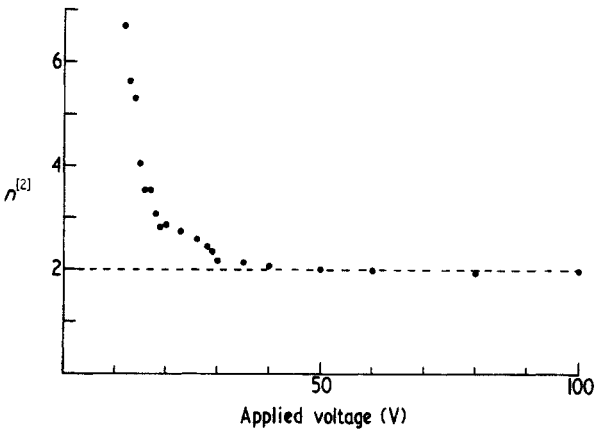

Figure 7. Second intensity moment as a function of applied voltage ($\theta = 21{\cdot}6°$, $W_0 = 11{\cdot}29\,\mu m$).

In this section the discussion has been limited to the second moment $n^{[2]}$. Higher moments were, in fact, calculated from the measured $P(n)$'s. These have been presented elsewhere (Jakeman and Pusey 1973a, b and Jakeman 1974) and will be discussed further in § 4.

3.3. Two-detector experiments—spatial correlations

The cross-correlation coefficient $\langle I_1(t)I_2(t)\rangle/\langle I_1\rangle\langle I_2\rangle$ between the intensities $I(t)$ detected by PMT's 1 and 2 was estimated experimentally by operating the correlator in the cross-correlation mode and measuring the initial value of the photocount temporal cross-correlation function, $\lim_{\tau\to 0}\langle n_1(0)n_2(\tau)\rangle/\langle n_1\rangle\langle n_2\rangle$. For the measurements to be described in this section a sample time $T = 10\,\mu s$ was used. Since this is again much shorter than the coherence time of the light, the measured correlation functions were essentially horizontal straight lines whose normalized value gave $\langle n_1 n_2\rangle/\langle n_1\rangle\langle n_2\rangle$. The 'Malvern' correlator requires a 'one-bit' signal for the time-delayed channel. In these experiments this was achieved by scaling the photocounts from one of the PMT's by a factor chosen large enough that the probability of occurrence of more than one scaled photocount in the sample time T was negligible (see eg Pusey and Goldburg 1971, Jakeman *et al* 1972, Koppel and Schaefer 1973). The technique of clipping (Jakeman and Pike 1969), commonly used to obtain one-bit signals from signals having Gaussian statistics, could not be used in this case, since the effects of clipping arbitrary non-Gaussian signals are unknown. Single-scaling, however, yields a direct measure of the *full* photocount correlation function.

Figures 8 and 9 show the cross-correlation coefficient as a function of the angular position of PMT 2, with PMT 1 placed at $\theta = 29{\cdot}1°$. The calculated beam waist W was $9{\cdot}46\,\mu m$, giving a corrected value of $12{\cdot}46\,\mu m$. The upper trace in each figure shows the situation for an applied voltage $V = 20$ V, whereas the lower trace is for $V = 100$ V. These curves show the expected general features. At 100 V the scattered light is expected to have Gaussian statistics (see § 3·2). The cross-correlation coefficient is expected to decay from 2 when the two detectors are superimposed to 1 when they are widely separated, with a spatial decay rate determined by W_0. The Gaussian data of figure 8

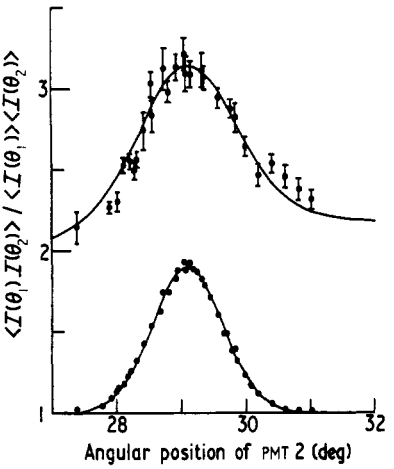

Figure 8. Cross correlation between intensities detected at two different scattering angles ($W_0 = 12{\cdot}46\,\mu m$). PMT 1 was fixed at $\theta_1 = 29{\cdot}1°$ and the position of PMT 2 was varied. The top trace is for $V = 20$ V and the full curve is equation (3) with $\xi = 2{\cdot}63\,\mu m$ and $\overline{\phi^2} = 45{\cdot}57\,rad^2$. The bottom trace is for $V = 100$ V.

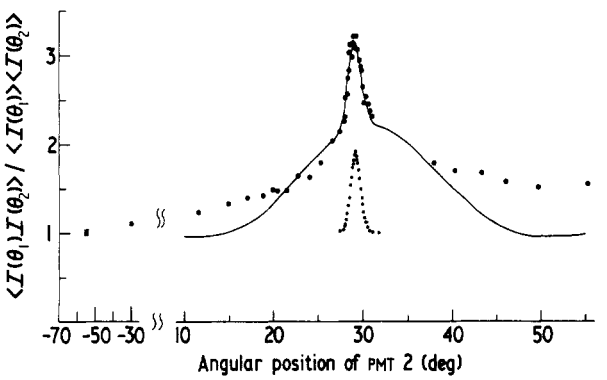

Figure 9. As for figure 8, spanning a larger range of angular separation of detectors.

are well fitted by the equation (the lower full curve)

$$\frac{\langle I_1 I_2\rangle}{\langle I_1\rangle\langle I_2\rangle} = 1 + 0{\cdot}91\exp\left(-\frac{k^2 W_0^2 v^2}{4}\right)$$

with $W_0 = 17\,\mu m$. It is not clear why the full Gaussian value of 2 was not observed. It is possible that, due to vertical displacement of the beam splitter, the two detectors were not truly superimposed at $v = 0$. This is a small effect, however, which was neglected in analysing the $V = 20$ V data. The experimental value of W_0, obtained by fitting the data to the above equation, is nearly twice the calculated value, indicating, not unexpectedly, a large degree of beam spreading at 100 V.

At 20 V the data clearly indicate the existence of two different spatial coherence lengths. The Gaussian term is evident leading to a decay of the correlation coefficient from about 3·1 to 2·1 over a spatial separation of about 2°. In addition there is a much slower decay from 2·1 towards one, corresponding to the non-Gaussian term in equation

(3). For the data at 20 V, some ten 100 s experimental runs were made for each position of PMT 2. The error bars in figure 8 indicate standard deviations obtained from these ten experimental values of the correlation coefficient. The upper full curve (in both figures) is equation (3), with the parameters $\xi = 2{\cdot}63\,\mu m$, $\overline{\phi^2} = 45{\cdot}57$ and $W_0 = 12{\cdot}46\,\mu m$. There is fairly good agreement between experiment and theory, with less than one third of the data points lying more than one standard deviation away from the theoretical line in the region of the Gaussian peak. However the data do appear to show slightly more asymmetry in this region than is predicted theoretically. The determination of whether this is a real effect or a small systematic error must await further experiments. For interest equation (3) was evaluated with $\xi = 2{\cdot}39\,\mu m$, $\overline{\phi^2} = 37{\cdot}51$ and $W_0 = 10{\cdot}46\,\mu m$. For the range of angular separations covered in figure 8, this line deviated from that shown in figure 8 by less than 5%, and it was impossible to claim that either set of parameters provided a better description of the data.

While figure 9 shows fairly good agreement between experiment and theory for small separations of the two detectors, there are significant differences at larger angular separations. This is almost certainly due to a weakness of the theoretical model discussed in § 4 of I—namely that it corresponds to a micro-area approach in which the regions of linearly changing phase are rather sharply defined, in the sense that there is little variation in their size. The discrepancy with theory manifest in figure 9 may therefore be interpreted as implying a wide range of 'facet sizes' on the wavefront emerging from the sample.

3.4. Temporal correlations

The time dependence of the light scattered by the liquid crystal at $V = 20$ V was analysed using single-scaled correlation. Three types of measurement were made: (i) the autocorrelation function of the photocurrent from one detector at $\theta = 29{\cdot}1°$ with a beam waist $W_0 = 12{\cdot}46\,\mu m$. This measurement should give the full correlation function of equation (4). (As expected, the results obtained by this measurement were indistinguishable from measurements of the cross correlation between two detectors when these were optically superimposed by means of the beam splitter.) (ii) A similar measurement using, however, a beam waist $W_0 \sim 500\,\mu m$. For such a measurement, the non-Gaussian term in equation (4) should be negligible, and only the Gaussian term should survive. (iii) The cross correlation, with $W_0 = 12{\cdot}46\,\mu m$, between two detectors, one at $\theta = 29{\cdot}1°$ and the other at $\theta \simeq 27{\cdot}5°$. Here, due to their different spatial coherence characteristics (figures 8 and 9), the Gaussian term should be negligible, but the non-Gaussian term hardly altered from measurement (i). Thus, after subtraction of the background terms, the results of measurement (ii), added to those of measurement (iii), should be almost the same as measurement (i).

Figure 10 shows the experimental results over the whole range of delay times spanned ($\sim 0{\cdot}5$ s). Figure 11 shows the short-time behaviour of the correlation functions (up to $\tau = 80$ ms). The general features of these results are as expected from the discussions in paper I. The Gaussian term shows a fairly rapid decay from about 2 to 1. The non-Gaussian term shows a much slower decay from about 2·2 to 1. The total correlation function is, apart from background terms, roughly the sum of these two components.

At short delay times an oscillation is evident in the total and Gaussian correlation functions but *not* the non-Gaussian term. This oscillation occurs at twice the frequency (50 Hz) of the voltage applied to the liquid crystal. It is perhaps not surprising that, at the relatively low applied voltage (20 V), the refractive index fluctuations of the sample

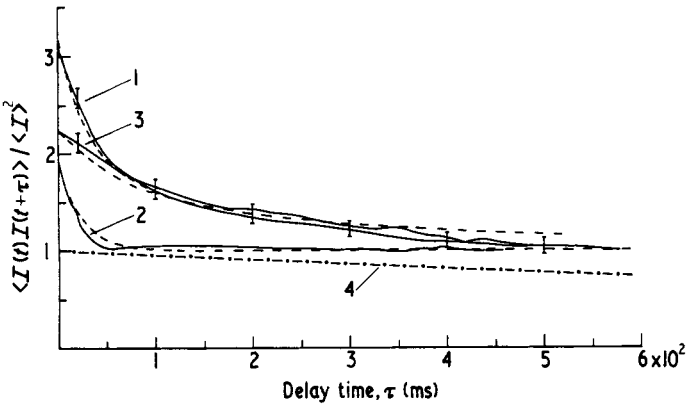

Figure 10. Temporal intensity correlation function of scattered radiation at $V = 20$ V. Curve 1: autocorrelation function of photocurrent from PMT 1 at $\theta_1 = 29{\cdot}1°$, $W_0 = 12{\cdot}46$ μm. Curve 2: autocorrelation function of photocurrent from PMT 1 at $\theta_1 = 29{\cdot}1°$, $W_0 \gtrsim 500$ μm. Curve 3: cross correlation between photocurrents of PMT 1 at $\theta_1 = 29{\cdot}1°$ and PMT 2 at $\theta_2 \simeq 27{\cdot}5°$, $W_0 = 12{\cdot}46$ μm. Full curves are the averages of several experiments. Broken curves are theoretical predictions (see text). The chain curve is the assumed temporal phase correlation function $\sigma(\tau)$.

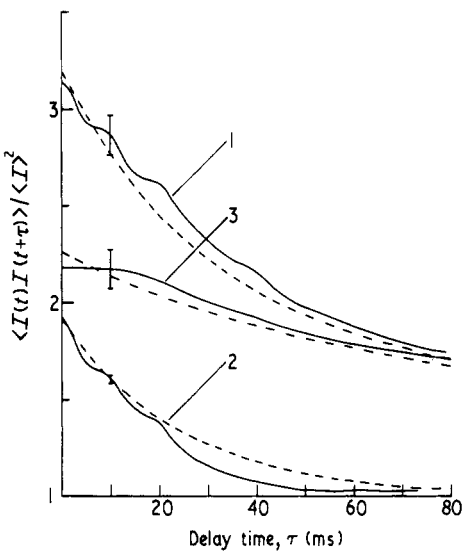

Figure 11. The same as figure 10, except spanning a smaller range of correlation delay times. Note that the ordinate scale starts at 1 in this figure.

follow to some extent the applied voltage. That the oscillation is observed in the Gaussian but not the non-Gaussian term indicates that the effect is relatively small—large enough to modulate the relative phases of two facets over an appreciable fraction of 2π, but not large enough to affect significantly the gross 'motion' of a single facet.

There are quite large errors in these measurements. Experimental run-times were typically 120 s, which, following the arguments of § 3.2, implies an error in the measurements of 4%, as an absolute minimum. The experimental data presented in figures 10

and 11 are the averages of five or so runs and the error bars represent typical run-to-run fluctuations. It should be noted, however, that, due to the high counting rates involved ($\sim 4 \times 10^4$ photocounts/s), the errors on data points in a single run were correlated over a delay range of roughly one coherence time. Thus, although in measurements of the total correlation function the run-to-run fluctuation in a given data point was large compared to the amplitude of the 100 Hz modulation, this latter was evident in individual runs, and therefore in their average.

According to the theory, the time dependences of both the Gaussian and non-Gaussian terms are determined by the temporal correlation function $\sigma(\tau)$ of the phase of the transmitted field (equation (4)). Lacking a detailed analysis of the mechanism of dynamic scattering, we have no theoretical predictions as to the form of $\sigma(\tau)$. It can be noted, however, that, for large $\overline{\phi^2}$, the time dependence of the Gaussian term is dominated by the short-time behaviour of $\sigma(\tau)$, which can presumably be written as a power series:

$$\sigma(\tau) = 1 - a|\tau| - b\tau^2 + \ldots, \tag{8}$$

where a, b etc are related to the characteristic fluctuation or coherence time(s) of the phase. If a is nonzero, the initial time dependence of the Gaussian term will be exponential $\exp(-2a\overline{\phi^2}\tau)$, whereas, if $a = 0$ but $b > 0$, the initial time dependence will have the form $\exp(-2b\overline{\phi^2}\tau^2)$, a Gaussian in τ with zero limiting slope as $\tau \to 0$. The data of figure 11 show a nonzero slope at $\tau = 0$ for the Gaussian term, indicating $a \neq 0$. A semi-log plot of these data (figure 12) shows, apart from the oscillations discussed above, the initial straight-line behaviour expected for an exponential in τ. There is in this plot, however, significant deviation from a straight line at larger τ implying that the quadratic term in equation (8) is not negligible.

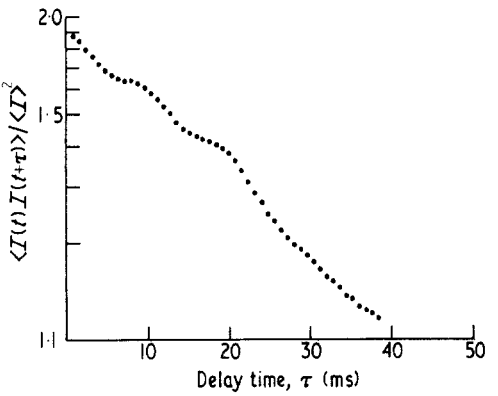

Figure 12. Semi-log plot of trace 2; figure 11.

Nevertheless, in the absence of theoretical predictions for $\sigma(\tau)$, there seems little point in attempting, at least with our data of fairly low precision, a detailed analysis keeping several terms in equation (8). Accordingly we took

$$\sigma(\tau) = 1 - \frac{|\tau|}{T_c} \qquad \tau \leqslant T_c. \tag{9}$$

(All our data are for τ considerably less than T_c.) The broken curves in figures 10 and 11 are equation (4) plotted for $\overline{\phi^2} = 45{\cdot}57$, $\xi = 2{\cdot}63\,\mu\text{m}$, $W_0 = 12{\cdot}46\,\mu\text{m}$ and $T_c = 2{\cdot}2\,\text{s}$

(measurements (i) and (iii)). The broken curve for measurement (ii) is

$$\frac{\langle I(0)I(\tau)\rangle}{\langle I\rangle^2} = 1+0{\cdot}92\exp[2\overline{\phi^2}(\sigma(\tau)-1)] \tag{10}$$

the result expected for $W_0 \gg \xi$, except for the incorporation of the factor 0·92 chosen to fit the data at $\tau = 0$. The failure of the data to reach the true Gaussian value of 2 is probably caused by incomplete spatial coherence at the detector due to the large illuminated region in this situation. It is seen from figures 10 and 11 that, with this choice of parameters, there is gratifyingly good agreement between experiment and theory. As expected from the discussion above, the experimental Gaussian term falls off more rapidly than predicted at long delay-time, and the non-Gaussian term appears to show a similar effect. Agreement would very likely be improved by inclusion of higher terms in equation (8). It should be emphasized, however, that an important feature demonstrated by these data is that a *single time-constant* T_c describes fairly well through equation (4) the behaviour of *both* the Gaussian and non-Gaussian terms.

The value 2·2 s for the fundamental coherence time of the phase fluctuations was chosen since it gave the best overall fit, as judged by eye, to the data. The phase correlation function $\sigma(\tau)$ with this value of T_c (equation (9)) is plotted in figure 12. It should be noted that at the value of τ (~ 100 ms) for which the Gaussian term has fallen to about 1 % of its value at $\tau = 0$, $\sigma(\tau)$ has only changed by about 5 %. This emphasizes the fact, mentioned above, that, at least for large $\overline{\phi^2}$, the time dependence of the Gaussian term is relatively insensitive to the form of $\sigma(\tau)$ being determined almost entirely by its short-time behaviour. On the other hand the non-Gaussian term is nonzero for a larger range of delay times and therefore over a larger range of variation of $\sigma(\tau)$. Thus $\sigma(\tau)$, which in many manifestations of a deep phase screen must be a quantity of fundamental interest, can be determined easily from the time dependence of the non-Gaussian term, provided that this can be measured with sufficient accuracy. The quantity T_c can be regarded as the 'lifetime' of a facet in the scattered phase front. It is encouraging to note that the visual observation of the 'lighthouse' effect mentioned in the introduction yields a characteristic time of the order of a second or two.

Finally, we note that, while at $V = 20$ V the Gaussian part of the temporal correlation function has a roughly exponential form, at higher applied voltages a flatter top to the curve is observed. At $V = 100$ V a bell-shaped curve characteristic of a Gaussian function of τ is found. In addition the coherence time of the correlation function decreases markedly with increasing applied voltage.

4. Concluding remarks

The results of § 3 indicate that, under the conditions of our experiment, MBBA in its dynamic scattering state can be described by the theories of a deep random phase screen. With two relatively minor exceptions the data presented are consistent with a joint-Gaussian emergent phase correlation function of the form

$$\langle\phi(\boldsymbol{r}, t)\phi(\boldsymbol{r}', t')\rangle = \overline{\phi^2}\left(1-\frac{|\boldsymbol{r}-\boldsymbol{r}'|^2}{\xi^2}\right)\left(1-\frac{|t-t'|}{T_c}\right)$$

for $|\boldsymbol{r}-\boldsymbol{r}'| \ll \xi$, $|t-t'| \ll T_c$. Here $\phi(\boldsymbol{r}, t)$ is the instantaneous deviation of the emergent

phase from its mean value at point $\boldsymbol{r}$ in the exit face of the liquid crystal layer. Three parameters $\overline{\phi^2}$, ξ and T_c then describe the data. The exceptions concern the spatial coherence of the non-Gaussian fluctuations in the scattered light at large angular separations, discussed in § 3.3, and their temporal coherence at large delay times, discussed in § 3.4.

Despite this agreement, questions remain unanswered. We have already stated (§ 2) that all our data were obtained from a single sample cell of liquid crystal. For this sample data were reproducible over a period of at least a year. However, a few measurements were made on a different sample within two days of its construction. Here significantly different results were obtained. Under conditions where the first sample gave a second intensity moment $n^{[2]}$ (equation (2)) of about 3·5, the second sample gave a value of about 5. In addition, the threshold voltage for the onset of dynamic scattering was about 6 V for the first sample and about 8 V for the second. These differences may be due to contamination of the liquid crystal by impurities such as water vapour permeating the epoxy resin used to seal the cell, or possibly impurities leached from the resin itself. In any case further experiments are needed to investigate these observations.

We now return to a consideration of the possible existence of and effects of amplitude fluctuations in the wavefront emerging from the liquid crystal layer. As mentioned in § 1, we can consider at least two types of amplitude fluctuation: 'propagation-induced' fluctuations due to interference at the exit face of rays having suffered different phase shifts on transit through the liquid crystal layer, and 'intrinsic' fluctuations due to the scattering of a fluctuating amount of energy into the orthogonal polarization. An estimate of the importance of propagation-induced fluctuations can obviously be obtained from the relative magnitudes of the beam spreading-parameter x (see § 3.2) and the phase correlation length ξ. For $x \ll \xi$, adjacent rays will pick up much the same phase shift on transit through the sample and propagation-induced amplitude fluctuations will be small. For $x \gg \xi$, however, rays arriving at some point in the exit face of the sample may have suffered totally different, uncorrelated, phase shifts and one might expect considerable propagation-induced amplitude fluctuations. For the experiments described above, x ($\simeq 3 \pm 2$ μm) and ξ ($\simeq 2{\cdot}6$ μm) are roughly equal so that the presence of propagation-induced amplitude fluctuations cannot be ruled out. With regard to intrinsic amplitude fluctuations, we have already mentioned (§§ 1 and 3.1) that the existence of appreciable scattered intensity in the HV configuration indicates that they are not entirely negligible.

Whatever their source, the amplitude fluctuations can be expected to have much the same temporal and spatial correlation properties as the phase fluctuations at the exit face of the sample and the only quantities which are likely to be strongly influenced by their presence are the single-interval statistics $P(n)$ of the scattered light (§ 3.2). We may expect the non-Gaussian parts of the factorial moments $n^{[m]}$ of $P(n)$ calculated on the assumption of phase fluctuations alone to be multiplied by the moments of the amplitude fluctuations. In a previous publication (Jakeman and Pusey 1973a) we have mentioned that the experimentally determined higher factorial moments indeed increase more rapidly with m than is predicted by consideration of phase fluctuations alone. There we assumed intrinsic amplitude fluctuations to be the only contributing factor, and, with the assumption that these fluctuations were log-normally distributed, calculated their effect. We note, however, that the theoretical values of $n^{[m]}$, $m > 2$, were not calculated exactly, but were obtained from the facet model (I, § 3.5). As discussed in I (§ 4) a limitation of this model is that uniform facet size is assumed. It can be argued

that fluctuations in facet size will lead to higher values of $n^{[m]}$. Thus, while the high experimental $n^{[m]}$ are almost certainly due in part to amplitude fluctuations, we cannot yet estimate their effect quantitatively. We note, however, that if we accept the over-estimated effect of intrinsic amplitude fluctuations given previously (Jakeman and Pusey 1973a), by shifting the data in figure 6 downward by roughly a factor of two, an interpretation in terms of phase fluctuations alone can be made. This yields values of ξ and $\overline{\phi^2}^{1/2}$ differing from those given by a factor $2^{1/4}$. Even this, then, is a relatively small effect.

Several other investigations of dynamic scattering by light scattering can be compared with our measurements. Using classical interferometric techniques, Bartolino *et al* (1973) have studied the spatial coherence properties of the transmitted light *in the near field*, yielding a direct measurement of the emergent phase correlation length ξ. These measurements, made on a 12·5 μm layer of MBBA, were limited to $\xi > 10\,\mu m$ and applied voltages $V < 10$ V. Nevertheless, extrapolation of their data (Bartolino *et al* 1973, figure 8) giving ξ as a function of V yields $\xi \simeq 3{\cdot}3\,\mu m$ at $V = 20$ V. This result compares favourably with our value $\xi \simeq 2{\cdot}6\,\mu m$, when account is taken of errors inherent in the extrapolation procedure and the different cell thickness used. Using the same interferometric technique, Scudieri *et al* (1974) have studied the spatial coherence of the *far-field* scattered light, finding, in qualitative agreement with our results, increasing spatial coherence over areas larger than the conventional (Gaussian) coherence area as the region of sample illuminated is decreased in size. In addition, using heterodyne light-beating methods, these authors measured the decay rate of Gaussian fluctuations in the far-field scattered radiation, and found it to be virtually independent of scattering angle. This result is in agreement with our theoretical predictions (equation (4), where no dependence on angle is predicted for the first term) and is in marked contrast to similar measurements in other materials where single-scattering theories apply (Scudieri *et al* 1974, Bertolotti *et al* 1972; see, also, § 1). Finally Bertolotti and Scudieri (1974; also Bertolotti 1974) have also observed departures from Gaussian single-interval statistics in the scattered light when small illuminated areas are used. They did not, however, give a quantitative analysis of their data.

An original motivation for the work reported in this paper was the hope of quantifying and perhaps improving, the visual appearance of dynamic scattering display devices (Jakeman and Pusey 1973b). It should be clear that the simple phase-screen model does not allow back-scattered radiation. Indeed our results indicate that, at least for relatively thin liquid crystal layers, the vast majority of the incident radiation is scattered into the forward hemisphere. What back-scattering is observed is probably due to reflection at the second liquid crystal–glass interface. The visual appearance of displays operated in a back-scattering configuration could presumably be improved by using a glass of high refractive index for the second enclosing plate (see also Heilmeier *et al* 1968). Of course increased non-specular back-scattered radiation in the on-state would then be accompanied by increased undesirable specular reflection in the off-state. Requirements for improved intrinsic back-scattering obviously include $\overline{\phi^2} > 2\pi$ and ξ as small as possible. Studies of the general type outlined in this paper could possibly aid in the search for materials having these characteristics.

Finally, taking a broader view, our work confirms that light-scattering studies in the non-Gaussian regime (illuminated region of size comparable to structure within the scatterer) can yield detailed information about the individual scatterers, not necessarily available from studies in the Gaussian regime (see, also, Pusey *et al* 1974, Schaefer 1974, Schaefer and Pusey 1972, Bluemel *et al* 1972, Bourke *et al* 1970).

Acknowledgments

We are grateful to Dr E P Raynes for providing the liquid crystal sample and to Dr E R Pike for valuable criticism of the manuscript.

References

Bartolino R, Bertolotti M, Scudieri F and Sette D 1973 *Appl. Opt.* **12** 2917
Bertolotti M, Daino B, Di Porto P, Scudieri F and Sette D 1971 *J. Phys.* A: *Gen. Phys.* **4** L97
—— 1972 *J. Phys., Paris* **33** C1 63
Bertolotti M and Scudieri F 1974 to be published
Bertolotti M 1974 *Photon Correlation and Light-Beating Spectroscopy* eds H Z Cummins and E R Pike (New York: Plenum Press) p 41
Bluemel V, Narducci L M and Tuft R A 1972 *J. Opt. Soc. Am.* **62** 1309
Bourke P J *et al* 1970 *J. Phys.* A: *Gen. Phys.* **3** 216
Briggs B H 1966 *Radio Sci.* **1** 163
Cantrell C D 1970 *Phys. Rev.* A **1** 672
Deutsch C and Keating P N 1969 *J. Appl. Phys.* **40** 4049
Haller I and Litster J D 1970 *Phys. Rev. Lett.* **25** 1550
Heilmeier G H, Zanoni L A and Barton L A 1968 *Proc. IEEE* **56** 1162
Jakeman E, Oliver C J and Pike E R 1970 *J. Phys.* A: *Gen. Phys.* **3** L45
Jakeman E, Oliver C J, Pike E R and Pusey P N 1972 *J. Phys.* A: *Gen. Phys.* **5** L93
Jakeman E and Pike E R 1969 *J. Phys.* A: *Gen. Phys.* **2** 411
Jakeman E, Pike E R and Swain S 1971 *J. Phys.* A: *Gen. Phys.* **4** 517
Jakeman E and Pusey P N 1973a *J. Phys.* A: *Math., Nucl. Gen.* **6** L88
—— 1973b *Phys. Lett.* **44A** 456
Jakeman E 1974 *Photon Correlation and Light-Beating Spectroscopy* eds H Z Cummins and E R Pike (New York: Plenum Press) p 75
Jakeman E and Pusey P N 1975 *J. Phys.* A: *Math. Gen.* **8** 369–91
Kogelnik H and Li T 1966 *Appl. Opt.* **5** 1550
Koppel D E 1971 *J. Appl. Phys.* **42** 3216
Koppel D E and Schaefer D W 1973 *Appl. Phys. Lett.* **22** 36
Little L T and Hewish A 1966 *Mon. Not. R. Astron. Soc.* **134** 221
Mandel L 1959 *Proc. Phys. Soc.* **74** 233
Oliver C J 1974 *Photon Correlation and Light-Beating Spectroscopy* eds H Z Cummins and E R Pike (New York: Plenum Press) p 151
Orsay Liquid Crystal Group 1969 *J. Chem. Phys.* **51** 816
Pike E R 1969 *Riv. Nuovo Cim.* **1** 277
Pusey P N and Goldburg W I 1971 *Phys. Rev.* A **3** 766
Pusey P N, Schaefer D W and Koppel D E 1974 *J. Phys.* A: *Math., Nucl. Gen.* **7** 530
Salpeter E E 1967 *Astrophys. J.* **147** 433
Schaefer D W and Pusey P N 1972 *Phys. Rev. Lett.* **29** 843
Schaefer D W 1974 *Laser Applications to Optics and Spectroscopy* eds S F Jacobs, M O Scully, M Sargent and J F Scott (Reading, Mass.: Addison-Wesley)
Scudieri F, Bertolotti M and Bartolino R 1974 *Appl. Opt.* **13** 181